A simple water clarity-turbidity index for marine and inland waters: Great Lakes case study

Guangming Zheng[1,2], Paul M. DiGiacomo[1]

[1]NOAA/NESDIS Center for Satellite Applications and Research, 5830 University Research Court, College Park, MD 20740, U.S.A.

[2]Earth System Science Interdisciplinary Center, University of Maryland Research Park, 5825 University Research Court, College Park, MD 20740, U.S.A.

Key Points:

- A framework to extract water quality information from satellite data is proposed.
- The approach is applicable to all water bodies and types ranging from the clearest to the most turbid, freshwater and marine.
- The approach is flexible and can be easily adapted for different regions and applications.

Corresponding author: Guangming Zheng, guangming.zheng@noaa.gov

Abstract

There are a plethora of satellite-derived water clarity and turbidity indicators to support the decision making of environmental managers and policy makers. However, water quality dynamic ranges addressed by these indicators can differ significantly, subjecting unsuspecting users to potential pitfalls. Here we propose a satellite water clarity-turbidity index (CTI) as a simplified way to capture major changes in water clarity/turbidity across all water types. This is achieved by merging three satellite-derived indicators, namely, the Secchi disk depth, the particulate backscattering coefficient, and the nephelometric turbidity, which are suitable for clear, intermediate, and turbid waters, respectively. Application to the Great Lakes shows that with one parameter, the CTI can illustrate major spatial and temporal patterns that are not entirely visible with each of the three original indicators alone, making it a convenient holistic assessment tool for water quality management.

1 Introduction

Water clarity and turbidity are important water quality indicators that can be estimated from satellite data using various proxy variables. Commonly used variables include the Secchi disk depth, Z_{sd}, the particulate backscattering coefficient, $b_{bp}(\lambda)$, diffuse attenuation coefficient of downwelling irradiance, $K_d(\lambda)$, and turbidity in nephelometric turbidity units (NTU), T_n (Zheng & DiGiacomo, 2017). It is important to note that no single variable fits all water types with respect to covarying with changes in water quality; each individual variable has an optimal dynamic range. For example, the Secchi Depth Z_{sd} is well suited for clear waters but its magnitude tends to diminish in turbid waters. With errors and uncertainties which are inherent to satellite data, highly turbid waters are practically indistinguishable using only Z_{sd}. For a similar reason, it is also difficult to evaluate turbidity of clear waters using the nephelometric turbidity T_n. Perhaps a good question to ask is, why estimate turbidity for waters with little turbidity, or clarity when there is essentially no clarity?

Therefore, effective application of these satellite products requires knowledge about their applicable dynamic range. This could overwhelm water quality managers and policy makers who may not have technical expertise. Since satellite data alone will not provide answer to all problems for environmental managers and policy makers, but are more likely used in conjunction with traditional field measurement programs (Schaeffer et al.,

2013), a simple but broadly applicable product merging multiple variables might be more useful for the decision making (Mouw et al., 2015). In practice, a smart decision-making framework could include a strategic plan made based on low-cost and timely satellite data to identify priority locations, followed by field sampling activities targeting the priority locations to provide more precise and legally compliant measurements, particularly at depth and also to provide parameters that cannot be measured from space (e.g., nutrients and pathogens). In this study, we develop such a product that addresses the turbidity/clarity of all water types ranging from the clearest to the most turbid waters by merging Z_{sd}, $b_{bp}(\lambda)$, and T_n. The efficacy of the new product is demonstrated using data from the Great Lakes which is the largest system of fresh surface water by total area in the world and water turbidity varies greatly in this region. Another motivation of using the Great Lakes as a case-study site is because the anthropogenic environment and aquatic ecosystems of the Great Lakes were historically impaired by pollution and invasive species; our product may help facilitate the restoration activities.

2 Data and Methods

2.1 Data

The remote-sensing reflectance, $R_{rs}(\lambda)$, data covering the Great Lakes region were obtained from three satellite missions: Visible Infrared Imaging Radiometer Suite (VIIRS)-SNPP (2011-2019), Moderate Resolution Imaging Spectroradiometer (MODIS)-Aqua (2002-2019), and MODIS-Terra (2000-2019). Daily Level-2 VIIRS-SNPP granule data with "science quality" were processed by the NOAA Ocean Color Science Team (reprocessing version, SCI_OC04.0_V1.21) and are available on the NOAA CoastWatch website (coastwatch.noaa.gov). Daily Level-2 MODIS-Aqua and -Terra data were obtained from the NASA's Goddard Space Flight Center Ocean Biology Processing Group using the Level 1&2 Browser on oceancolor.gsfc.nasa.gov. Data were reprocessed in 2018 (version "R2018.0"). Both VIIRS and MODIS data were produced with the atmospheric correction using the near-infrared bands as a basis for making the "black-pixel" assumption. To avoid ice contamination, most data used in this study were collected during warm seasons from May to September unless otherwise noted.

As preprocessing, data were screened to remove quality issues and then gridded. Specifically, we rejected pixels flagged as high sun or sensor zenith angles, or high glint.

In addition, the daily Level-2 data granules were reprojected into gridded format at 750-m (VIIRS) and 1000-m (MODIS) resolutions, respectively, and monthly composites for each individual band were calculated as the mean of all gridded daily images in each month. The final product of this preprocessing is monthly 2-D arrays of the VIIRS $R_{rs}(\lambda)$ data at 410, 443, 486, 551, 638, and 671 nm, and MODIS $R_{rs}(\lambda)$ data at roughly identical bands, i.e., 412, 443, 469, 488, 547, 645, and 667 nm. Other MODIS ocean color bands were excluded from further calculations. Note that the VIIRS 638-nm band is not a regular ocean color band, but an "I-band" with 2 times higher spatial resolution and roughly 1/3 signal-to-noise ratio (SNR). So each $R_{rs}(638)$ value is aggregated from 4 I-band pixels and in this process its SNR is somewhat enhanced.

2.2 Methods

We propose a clarity-turbidity index (CTI) product to provide a simple, qualitative measure of overall water quality across essentially all natural waters, ranging from the clearest to the most turbid, freshwater and marine. The CTI can be determined based on three satellite-derived variables, namely Z_{sd}, $b_{bp}(550)$, and T_n which account for water quality variability of the clearest, the intermediate, and the most turbid waters, respectively.

There are many formulas to derive Z_{sd} from $R_{rs}(\lambda)$ (e.g., Doron et al., 2011; Lee et al., 2015, and references cited therein). Here we used a formula based on the one given by Lee et al. (2015):

$$Z_{sd} = \frac{1}{2.5K_d(\lambda_{min})} \ln\left(\frac{\mid 0.14 - R_{rs}(\lambda_{min}) \mid}{0.013}\right) \tag{1}$$

, where $K_d(\lambda)$ is the vertically averaged spectral diffuse attenuation coefficient, and λ_{min} is the light wavelength with minimum $K_d(\lambda)$, i.e., where light can penetrate the deepest into the water column. Also following Lee et al. (2015), $K_d(\lambda)$ was calculated from the spectral light absorption, $a(\lambda)$, and backscattering coefficients, $b_b(\lambda)$, which were calculated with the Quasi-Analytical Algorithm (QAA) version 6 (Lee et al., 2013).

The particulate $b_{bp}(550)$ is calculated simply by subtracting the pure water contribution, $b_{bw}(550)$, from the total $b_b(550)$. Note that the 550 nm here is a nominal band name referring to the 551 nm for VIIRS and 547 nm for MODIS. The $b_{bw}(550)$ is calculated with the Water Optical Properties Processor (WOPP) developed by Rottgers et al. (2011). In this calculation water salinity was set to zero, and water temperature

to 10 °C which is close to the medians of monthly whole-lake average temperature of individual Great Lakes from May to September (see coastwatch.glerl.noaa.gov/statistic/).

To calculate turbidity in nephelometric units, T_n, we used a formula based on the magnitude of $R_{rs}(645)$ (or 638 nm for VIIRS) from Dogliotti et al. (2015):

$$T_n = \frac{228.1\pi R_{rs}(645)}{1 - \pi R_{rs}(645)/0.1641} \tag{2}$$

We also examined the use of T_n derived from reflectance at near-infrared bands to account for more turbid waters but found it unnecessary because such waters are rare in the Great Lakes. However, this may be needed for application in more turbid waters elsewhere.

Given Z_{sd}, $b_{bp}(550)$, and T_n, the CTI is determined based on threshold values of these variables as illustrated in Table 1 and Fig. 1. Figure 1 shows the distribution of all monthly VIIRS data used in this study which comprise over two million samples. The MODIS data show similar patterns except that the T_n rarely exceeds 60 NTU (not shown). The first step is to separate the two endmember groups, i.e., clear waters and turbid waters. This is important because turbidity indicator T_n diminishes in clear waters and clarity indicator Z_{sd} diminishes in turbid waters, and as they diminish, they also lose the dynamic range to capture the variability of water quality (see right end of blue points and left end of red points in Fig. 1). Based on the VIIRS data distribution, two threshold values of $b_{bp}(550)$, 0.01 and 0.1 m^{-1}, were selected to broadly categorize a given pixel into clear (CTI $\leq$4), intermediate (CTI 5), or turbid waters (CTI $\geq$6). The value of 0.01 m^{-1} happens to intercept with the upper bound of Z_{sd}–$b_{bp}(550)$ distribution at Z_{sd} $\approx$10 m, whereas the value of 0.1 m^{-1} happens to intercept with the upper bound of T_n–$b_{bp}(550)$ distribution at T_n $\approx$15 NTU. Therefore Z_{sd}=10 m is used as a threshold value to further separate the clearest (CTI$\leq$3) from the transitional clear-intermediate waters (CTI=4), and T_n =15 NTU is used to separate the intermediate-turbid (CTI=6) from the most turbid waters (CTI$\geq$7). For the clearest waters (CTI 1 through 3), the CTI is based solely on Z_{sd} with threshold values of 15 and 20 m, respectively; whereas for the most turbid waters (CTI 8 through 11), it is based solely on T_n with threshold values of 30, 60, 100, 200, and 500 NTU, respectively. There are relatively few data points beyond 200 NTU so they were not shown in Fig. 1 to better illustrate other CTI indices.

The choices of these threshold values may make the CTI approach appear arbitrary; nevertheless, it is the framework merging Z_{sd}, $b_{bp}(550)$, and T_n together that is important. The CTI approach is essentially a discretization, or data binning, of the three commonly used water clarity and turbidity variables. It transforms quantitative into qualitative information, while distilling and preserving dominant water quality information out of an overwhelmingly large amount of data, making it suitable for water quality managers and policy-makers to readily grasp general trends and patterns in both space and time. In addition, the way CTI is defined makes it a flexible approach. First, its applicable range of clarity/turbidity can be easily expanded; it can cover much clearer (e.g., oceanic waters with Z_{sd} as deep as 70 m, Gieskes et al., 1987; Doron et al., 2011; Lee et al., 2018) and much more turbid waters (e.g., T_n over 1000, Dogliotti et al., 2015). Second, the choices of threshold values are flexible; users can easily change these thresholds as they see fit and easily trace each CTI back to the ranges of Z_{sd}, $b_{bp}(550)$, and T_n through Table 1. In essence, the CTI provides a one-number metric for water quality managers and policy-makers to make quick evaluations without having to worry about technical details, particularly for regions where turbidity variation is large.

3 Results and Discussion

Using the approach discussed above we mapped out the CTI for the Great Lakes using $R_{rs}(\lambda)$ data from VIIRS-SNPP, MODIS-Aqua and -Terra, and made monthly composites for each sensor. Compared with Z_{sd}, $b_{bp}(\lambda)$, and T_n individually, the CTI product exhibits a broader range of variability. Taking VIIRS data in Arpil 2018 for example (Fig. 2), among the three original variables the clearest waters in central Lake Huron (white dashed circles) can only be seen in the Z_{sd} map, the most turbid waters in Lake Erie (black dashed circles) can only be seen in the T_n map, whereas the $b_{bp}(551)$ map only highlights turbidity changes in moderately turbid waters (e.g., the Saginaw Bay, gray dashed cicles). In contrast, the CTI map shows all main features across all water types ranging from the clearest to the most turbid.

Next, we examined the consistency of CTI product derived from VIIRS-SNPP, MODIS-Aqua and -Terra by comparing the CTI values derived from the 3 different sensors. For brevity we selected one month from each season (spring, summer, and fall) and calculated the lakewide average CTI. Figure 3 shows that the agreement among the three sensors is generally very good particularly for the two MODIS sensors which exhibit almost

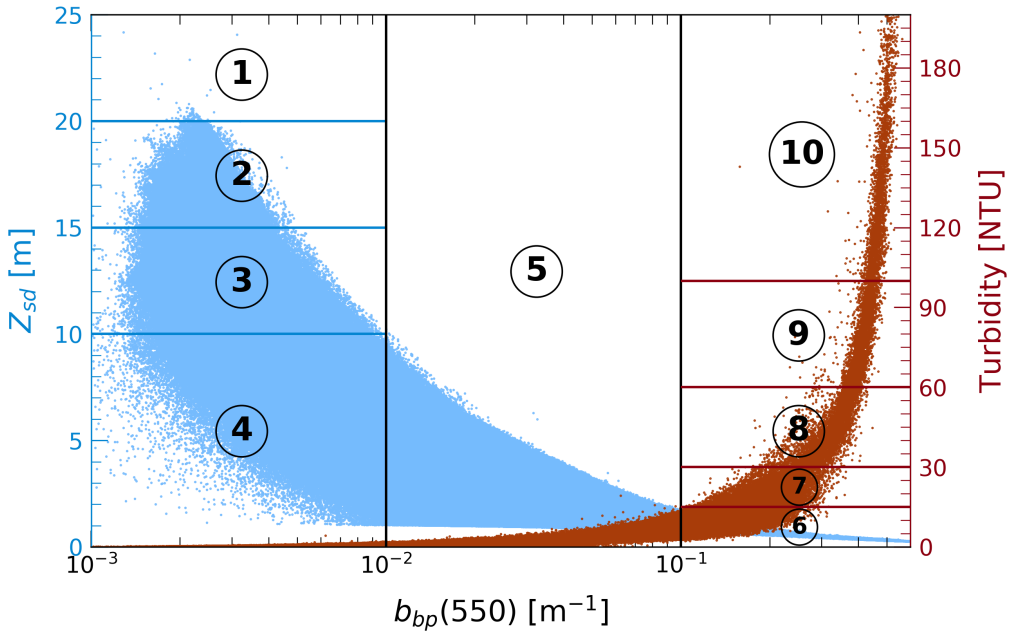

Figure 1. VIIRS-SNPP monthly averaged Z_{sd}, $b_{bp}(550)$, and T_n data in the Great Lakes during 2012-2019 overlaid with clarity-turbidity indices (denoted by circled numbers). See Table 1 for numerical definitions.

Table 1. Definitions of clarity-turbidity indices based on satellite-derived Z_{sd}, $b_{bp}(550)$, and T_n. Blank means the corresponding variable is not used to define a specific index.

Index	Water type	$Z_{sd}[m]$	$b_{bp}(550)[m^{-1}]$	Turbidity [NTU]
1	Clear-3	20−25		
2	Clear-2	15−20		
3	Clear-1	10−15		
4	Clear-Intermediate	0−10	<0.01	
5	Intermediate		0.01−0.1	
6	Intermediate-Turbid		>0.1	<15
7	Turbid-1			15−30
8	Turbid-2			30−60
9	Turbid-3			60−100
10	Turbid-4			100−200
11	Turbid-5			200−500
12	Turbid-6			>500

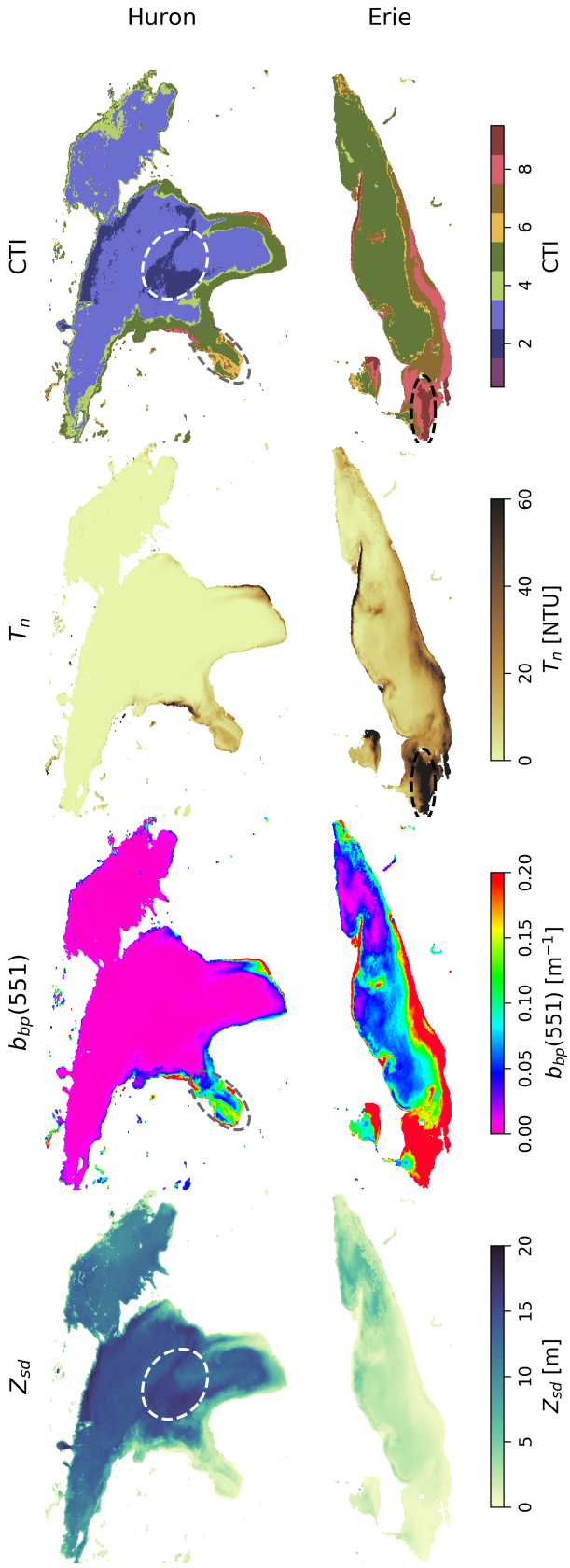

Figure 2. Comparison between maps of VIIRS-derived Z_{sd}, $b_{bp}(\lambda)$, and T_n and the merged CTI product using Lakes Huron and Erie in April 2018 as an example.

identical results. VIIRS-derived CTI values are systematically larger than the MODIS counterparts but they generally follow the same trend. There are a few outliers such as Lake Superior in September 2014 and Lake Ontario in September 2015, which are associated with significantly different spectral shapes in VIIRS- and MODIS-derived $R_{rs}(\lambda)$. We did a sensitivity test (not shown) and found that the different spectral shapes are associated with different atmospheric correction schemes. Overall, the results suggest that for clear and intermediate waters the CTI can be considered independent from sensor, algorithm, and data-processing system. For turbid waters the VIIRS- and MODIS-derived CTIs can be significantly different owing to the smaller dynamic range exhibited in the MODIS 645-nm band.

Figure 3 also shows that from the whole-lake standpoint, water quality in Lakes Michigan and Huron exhibits significant decadal changes. In particular, dramatic CTI drop occurred around 2004, consistent with previous studies (e.g. Binding et al., 2015). Average CTI in May dropped from >4 in 2002−2003 to ∼3.5 in 2005 for Lakes Michigan and Huron (Fig. 3D,G). Average CTI in Lake Michigan dropped even more significantly in September than in May from >4.5 in 2001 to ∼3.5 in 2005 (Fig. 3F), but the same trend did not happen in Lake Huron. Another significant trend is found in July, when CTI kept dropping since 2000, reached the minimum in 2012 with a total drop of ∼0.8, and bounced back by a total of ∼0.7 as of 2019 (Fig. 3E,H). A similar trend was also found in Lake Superior in May (Fig. 3A), although the magnitude of variation is much smaller. Otherwise, CTI changes in the other three lakes, i.e., Lakes Superior, Erie, and Ontario over the past two decades (2000-2019) are mostly associated with interannual variability. Interestingly, Lake Ontario exhibits both the largest (in September, Fig. 3O) and the smallest (in July, Fig. 3N) interannual variability.

To further examine spatial patterns of water quality changes, we obtained quinquennial CTI maps using mean Z_{sd}, $b_{bp}(550)$, and T_n calculated every five years (Fig. 4). For this analysis we used only MODIS-Terra data which provides the longest time record (2000−2019). Note that MODIS-derived T_n tends to be underestimated at higher turbidity levels compared with VIIRS. However, this is a minor issue for the purpose of this study because very turbid waters only account for a negligible portion of the Great Lakes. Figure 4 confirms that the most significant change in CTI occurred in Lake Michigan and Huron and between the two periods of 2000−2004 and 2005−2009. Most areas in Lakes Michigan and Huron underwent a CTI drop by 1, and the biggest drop occurred

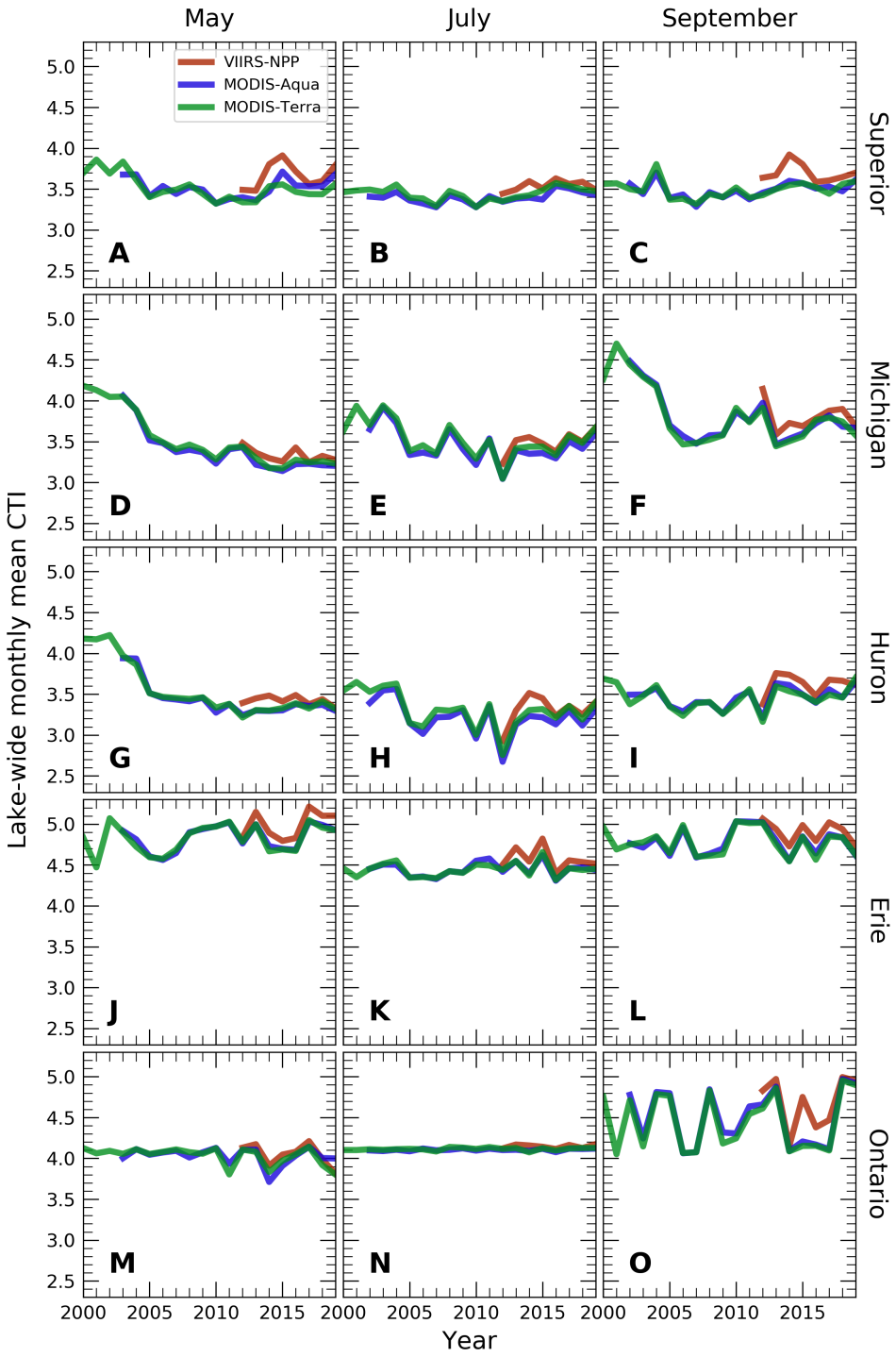

Figure 3. Lake-by-lake monthly mean clarity-turbidity index from 2000 to 2019 for May, July, and September.

in September in central southern Lake Michigan with a CTI drop by 2, from 5 (intermediate) to 3 (clear-1) (Fig. 4C,F). After this significant drop in water turbidity, Lake Huron and southern Lake Michigan continued to clear up during 2010−2019 whereas CTI of northern Lake Michigan stabilized. An intriguing spatial pattern is the decrease in CTI at relatively shallow locations in May. For example, the location of the clear waters with CTI = 2 in Lakes Michigan and Huron (dark blue in Fig. 4G,J) matches roughly with shallow bathymetry contours (not shown). This pattern might be associated with higher fraction of the water column cleared per day by invasive dreissenid mussels (Rowe et al., 2015), and in particular by quagga mussels in Lake Michigan (Nalepa et al., 2020) and Huron (Nalepa et al., 2018). The relationship between CTI and invasive mussels needs to be further investigated in future studies.

4 Summary

The CTI developed here is a simple approach to make an approximate evaluation of water turbidity or clarity for any type of optically deep water body, i.e., as long as the water-leaving light is unaffected by reflection off the water bottom. It allows the evaluation of water quality to be "approximately right", as opposed to "precisely wrong" which may result from the adoption of a variable that is inappropriate for the waters of interest. Application of this approach to satellite data essentially generates dynamic water quality thematic maps. In this study, we show that this approach allows the depiction of spatial gradients and temporal trends of water quality in the Great Lakes, and major turbidity drops in Lake Michigan and Lake Huron around 2004, a timing that matches the start of lake-wise infestation of invasive dreissenid mussels. We expect the CTI to be a useful tool for many other water bodies around the world, particularly for regions where water clarity/turbidity spans a great range, and recommend it to water quality managers and policy-makers whose intention is to seek holistic understanding from satellite data rather than conducting detailed quantitative analyses with them.

Acknowledgments

This work was supported by the Great Lakes Restoration Initiative (GLRI). Datasets for this research are freely available from coastwatch.noaa.gov and oceancolor.gsfc.nasa.gov, for which we are grateful. The contents of this article are solely the opinions of the au-

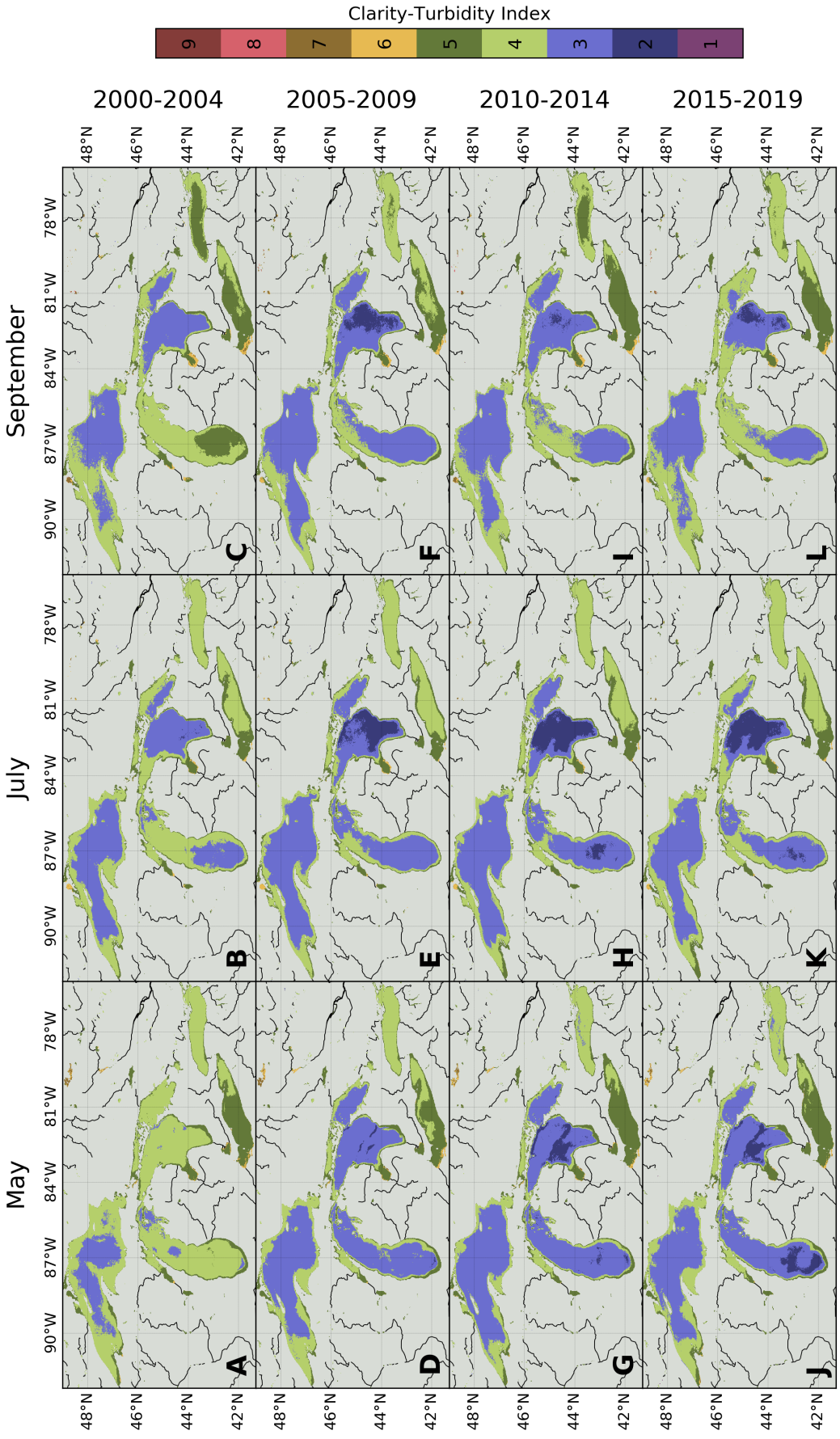

Figure 4. Quinquennial climatology of water clarity-turbidity index of the Great Lakes across spring, summer, and fall.

thors and do not constitute a statement of policy, decision, or position on behalf of the NOAA or the U.S. Government.

References

Binding, C. E., Greenberg, T. A., Watson, S. B., Rastin, S., & Gould, J. (2015). Long term water clarity changes in north america's great lakes from multi-sensor satellite observations. *Limnology and Oceanography*, *60*(6), 1976-1995. doi: 10.1002/lno.10146

Dogliotti, A., Ruddick, K., Nechad, B., Doxaran, D., & Knaeps, E. (2015). A single algorithm to retrieve turbidity from remotely-sensed data in all coastal and estuarine waters. *Remote Sensing of Environment*, *156*, 157 - 168. doi: 10.1016/j.rse.2014.09.020

Doron, M., Babin, M., Hembise, O., Mangin, A., & Garnesson, P. (2011). Ocean transparency from space: Validation of algorithms estimating secchi depth using meris, modis and seawifs data. *Remote Sensing of Environment*, *115*(12), 2986 - 3001. doi: 10.1016/j.rse.2011.05.019

Gieskes, W. W. C., Veth, C., Woehrmann, A., & Graefe, M. (1987). Secchi disc visibility world record shattered. *Eos, Transactions American Geophysical Union*, *68*(9), 123-123. doi: 10.1029/EO068i009p00123-01

Lee, Z., Arnone, R., Boyce, D., Franz, B., Greb, S., Hu, C., ... others (2018). Global water clarity: continuing a century-long monitoring. *Eos*, *99*. doi: 10.1029/2018EO097251

Lee, Z., Hu, C., Shang, S., Du, K., Lewis, M., Arnone, R., & Brewin, R. (2013). Penetration of uv-visible solar radiation in the global oceans: Insights from ocean color remote sensing. *Journal of Geophysical Research: Oceans*, *118*(9), 4241-4255. doi: 10.1002/jgrc.20308

Lee, Z., Shang, S., Hu, C., Du, K., Weidemann, A., Hou, W., ... Lin, G. (2015). Secchi disk depth: A new theory and mechanistic model for underwater visibility. *Remote Sensing of Environment*, *169*, 139 - 149. doi: 10.1016/j.rse.2015.08.002

Mouw, C. B., Greb, S., Aurin, D., DiGiacomo, P. M., Lee, Z., Twardowski, M., ... Craig, S. E. (2015). Aquatic color radiometry remote sensing of coastal and inland waters: Challenges and recommendations for future satellite missions.

Remote Sensing of Environment, *160*, 15 - 30. doi: 10.1016/j.rse.2015.02.001

Nalepa, T. F., Burlakova, L. E., Elgin, A. K., Karatayev, A. Y., Lang, G. A., & Mehler, K. (2020). *Abundance and biomass of benthic macroinvertebrates in lake michigan in 2015, with a summary of temporal trends.* Ann Arbor, Michigan. (Technical Memorandum) doi: 10.25923/g0d3-3v41

Nalepa, T. F., Riseng, C. M., Elgin, A. K., & Lang, G. A. (2018). *Abundance and distribution of benthic macroinvertebrates in the lake huron system: Saginaw bay, 2006-2009, and lake huron, including georgian bay and north channel, 2007 and 2012.* Ann Arbor, MI. (Technical Memorandum) doi: 10.25923/aqe2-ma69

Rottgers, R., Doerffer, R., McKee, D., & Schonfeld, W. (2011). *Algorithm theoretical basis document: The water optical properties processor (wopp)* (Tech. Rep.). Tech. rep., Helmholtz-Zentrum Geesthacht, University of Strathclyde, Geesthacht.

Rowe, M. D., Obenour, D. R., Nalepa, T. F., Vanderploeg, H. A., Yousef, F., & Kerfoot, W. C. (2015). Mapping the spatial distribution of the biomass and filter-feeding effect of invasive dreissenid mussels on the winter-spring phytoplankton bloom in lake michigan. *Freshwater Biology*, *60*(11), 2270-2285. doi: 10.1111/fwb.12653

Schaeffer, B. A., Schaeffer, K. G., Keith, D., Lunetta, R. S., Conmy, R., & Gould, R. W. (2013). Barriers to adopting satellite remote sensing for water quality management. *International Journal of Remote Sensing*, *34*(21), 7534-7544. doi: 10.1080/01431161.2013.823524

Zheng, G., & DiGiacomo, P. M. (2017). Uncertainties and applications of satellite-derived coastal water quality products. *Prog Oceanogr*, *159*, 45 - 72. doi: 10 .1016/j.pocean.2017.08.007